IVYSPRING INTERNATIONAL PUBLISHER

Theranostics

Research Paper

Tumor-selective dye-based histological electrophoresis enables intraoperative tumor diagnosis via tumor-specific enhancement

✉ ✉ ✉ ✉ ✉

Received: 2024.10.19; Accepted: 2024.12.09; Published: 2025.01.06

Abstract

Solid tissue biopsy is fundamental in guiding surgeons during intraoperative and peri-operative management of cancer patients. However, conventional histopathologic methods depend heavily on the expertise of trained pathologists, facing challenges in accuracy and efficiency.

Methods: Here, we show that unbiased labeling of proteins within tissue sections using tumor-selective dyes enhances tumor-specific signals, enabling robust and accurate differentiation of tumors from normal tissues in less than 45 min. This diagnostic approach combines a tumor-selective dye labeling strategy and a three-dimensional (3D) histological electrophoresis separation strategy to visualize protein differences between tissues and exclude off-target interference.

Results: We successfully diagnose and delineate malignant tissue from frozen and fresh surgical specimens from 34 patients across six types of cancer (mean AUC = 0.93). Furthermore, we apply this method to distinguish different histological characteristics in liver cancer surgical specimens, as well as identify and quantify the degree of inflammation in tumor-surrounding tissues.

Conclusion: This rapid, accurate, unbiased, and marker-free approach may enhance intraoperative detection of multiple types of tumor specimens.

Introduction

in vivo *ex vivo* *In vivo*

Figure 1 and S1

Figure 1 and S1

in vivo

ex vivo

Figure S2

Figure S2B

Figure S3

Figure 1A and S1A

Results and Discussion

Analysis of tumor-selective dye@protein signals and off-target signals in different tumor types

Figure 1B-H

P **Figure S1B**

Figure S1A

R

Figure S4A **Figure 1H** **Figure 1I** **and S1C**

Figure S1B

R **Figure 1C** *R*

Figure 1D *R* *R*

Figure 1F **Figure 1I**

Figure 1A and S1A, D

Figure 1A and S4B-G *P* **Figure S1B**

Figure S1A

R

Figure 1G **Figure 1I**

P

Figure 1. Protocol for evaluating the tumor identification effect of tumor-selective dyes. (A) Schematic workflow illustrating the concept of distinguishing tumors from surgical specimens via tumor-selective dye (IR-780) labeled tissue lysate and tissue sections, created with BioRender.com. For six types of prevalent tumor (liver, thyroid, breast, pancreas, bile duct, and cervix), the signals of IR-780@proteins in tumor tissue lysate are notably higher than in normal tissue lysate, enabling reliable tumor identification. However, when IR-780 is applied to tissue sections, the signals quantified from tumor regions are not consistently greater than that quantified from normal tissue regions, suggesting the influence of off-target signals in the tissue section staining protocol. (B) H&E analysis of nuclei density in the six types of tumor and their corresponding normal tissues (liver, n = 7; cervix, n = 6; bile duct, n = 5; pancreas, n = 5; thyroid, n = 6; breast, n = 9). (C-H) Correlation of the staining intensity of IR-780-labeled tissue sections and the nuclei density of tissue sections for liver (C), pancreas (D), cervix (E), thyroid (F), bile duct (G), and breast (H). Trendlines are shown for tumor (color-coded) 9 0Tw [illegible]

Tumor-selective dye@proteins identified by 3D histological electrophoresis distinguishes tumors from normal tissues

Figure 2A

Figure 2B

Figure 2C

and S5

Figure 2C and S5

in vivo *ex vivo*

Figure 2E-F and 3A-C

Figure 2D

Figure 3D

β (β

Figure S6

Figure S7 **Figure S8A-C**

Figure S2C

780@β

Figure S2C

P

Figure 2G

Figure 3E-G

Δ

Figure 3F

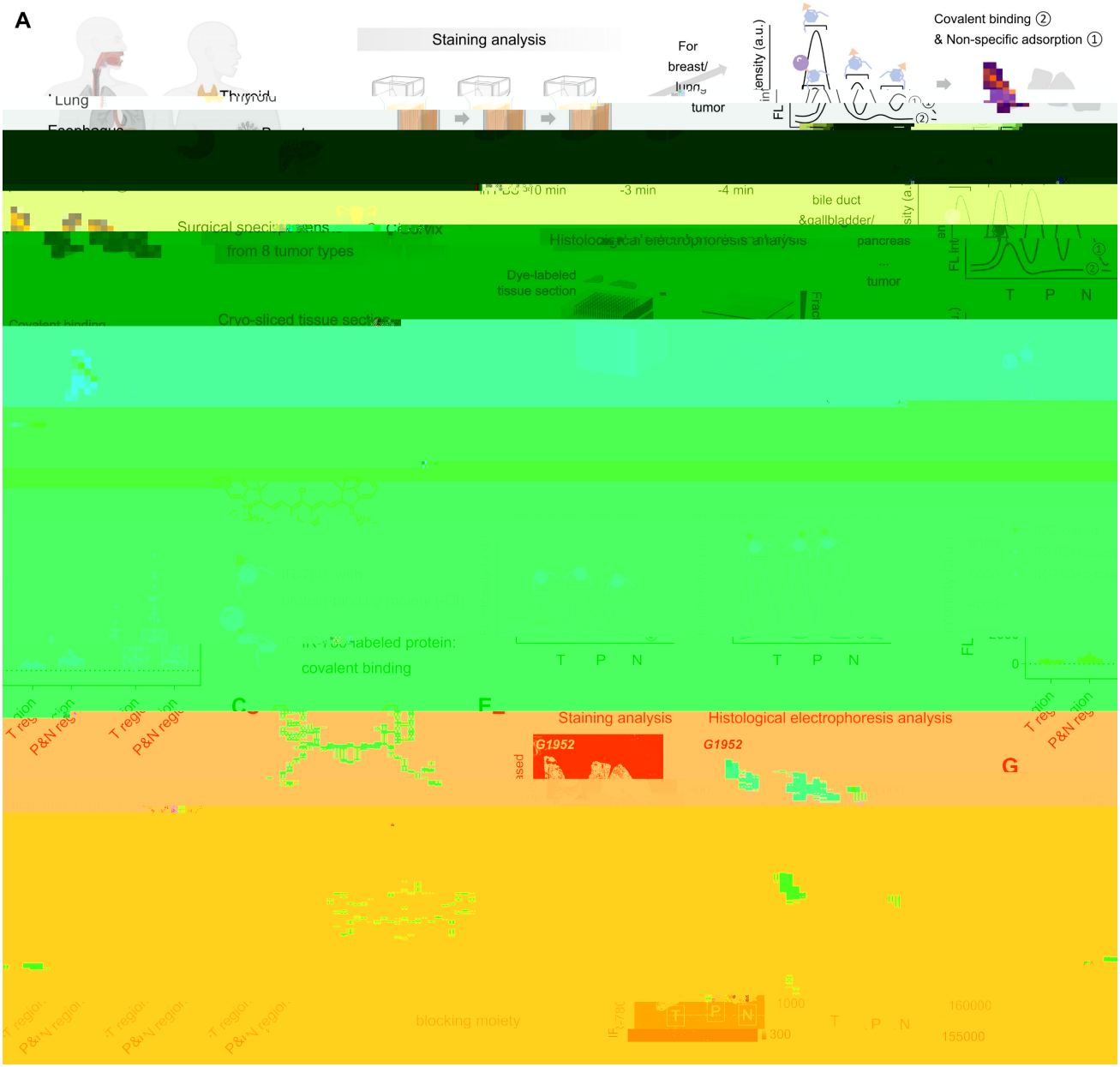

Figure 2. Purification of non-specific signals after tumor-selective dye staining by histological electrophoresis. (A) Schematic representation of the identification of histological types by covalent binding signals within tissue sections. Comparison of signals collected after IR-780-based staining analysis and IR-780-based histological electrophoresis analysis. The signals after staining analysis are derived from dyes that covalently bind to proteins within tissue sections and dyes that are non-specifically adsorbed to tissue sections. The signals after histological electrophoresis analysis are derived from dyes that covalently bind to proteins within tissue sections. (B) Chemical structure of IR-780 and schematic representations of IR-780 and IR-780-labeled protein. (C) Chemical structures and schematic representations of ICG and IR-780Ac. The binding behavior of ICG and IR-780Ac to proteins is different from that of IR-780 to proteins. Due to the absence of binding sites, ICG and IR-780Ac are unable to form stable covalent bonds with proteins. (D-G) Comparison of ICG-/IR-780-/IR-780Ac-based staining analysis and ICG-/IR-780-/IR-780Ac-based histological electrophoresis analysis in the liver cancer specimens from 3 patients (G1952, G0211, and S0002, **Table S1**). (D) Comparison of signals collected after staining analysis and histological electrophoresis analysis based on ICG and IR-780Ac. (E) Fluorescence intensity image describes staining analysis results. Heat map describes histological electrophoresis analysis results. The co-localization of H&E staining results and histological electrophoresis analysis results of tissue sections to describe the spatial distribution and abundance of IR-780 covalently bound proteins in tissue sections. Heat map represents the total signal of protein fractions after histological electrophoresis separation (fractions 1 to 8). (F and G) Plots of the signal intensity of multiple ROIs in tumor region and paracancerous and normal region after ICG-/IR-780-/IR-780Ac-based staining analysis (The number of ROIs is five, and the size of ROIs is 1 mm × 1 mm, F) and ICG-/IR-780-/IR-780Ac-based histological electrophoresis analysis (ROIs: n > 10, G). Top right of (G): Plot of the signal intensity of ROIs in tumor region and paracancerous and normal region after IR-780-based histological electrophoresis analysis after excluding signals of the necrotic region from G0211. Significant differences in signal intensity are observed between the tumor region and paracancerous and normal region (*****P* < 0.0001).

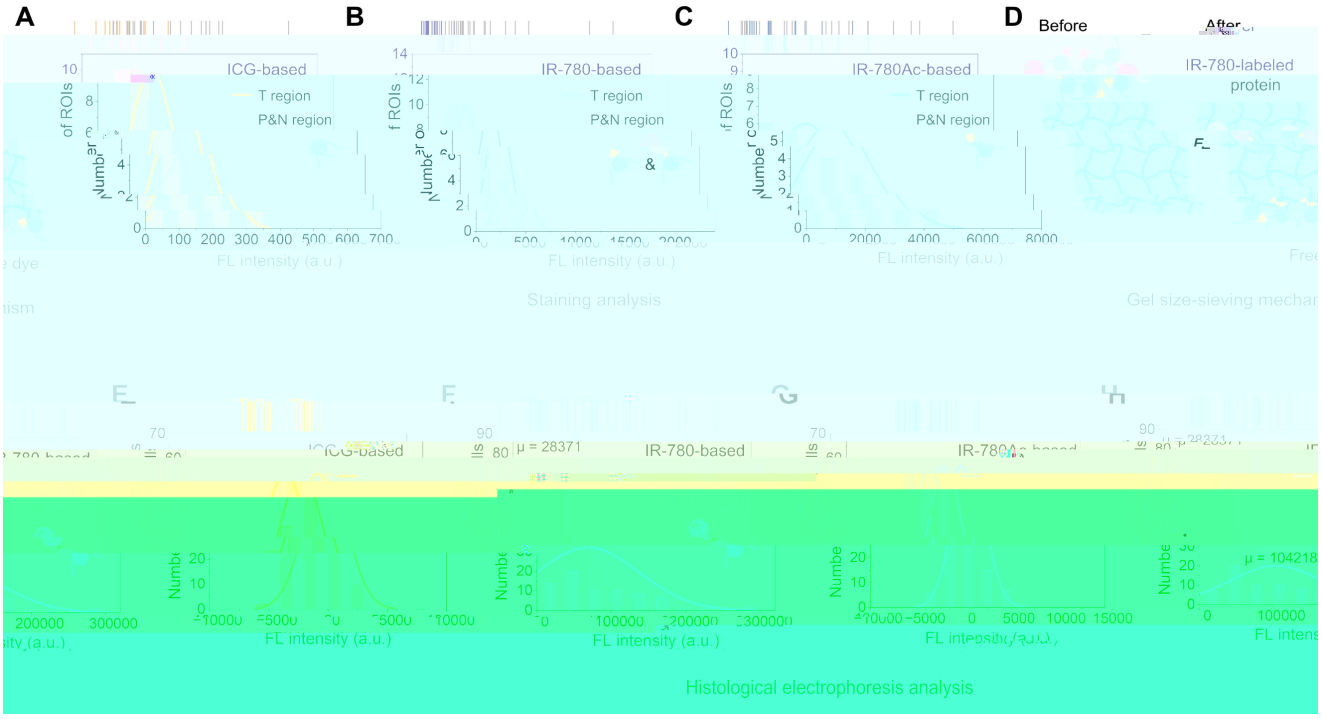

Figure 3. Illustrative plots of covalent binding signals in different regions within liver cancer tissue sections. (A-C) Histograms of signals after ICG-based (A), IR-780-based (B), and IR-780Ac-based (C) staining analysis in tumor region and paracancerous and normal region from the same tissue section of liver cancer specimen. (D) Schematic representation of the gel size-sieving mechanism for free dye removal. (E-H) Histograms of signals after ICG-based (E), IR-780-based (F), and IR-780Ac-based (G) histological electrophoresis analysis in tumor region and paracancerous and normal region from the same tissue section of liver cancer specimen. (H) Histogram reflects the signal distribution after IR-780-based histological electrophoresis analysis after excluding the necrotic region signals (from G0211).

Figure S10A-E

Figure 2G and S8

Figure S10F

Figure S9A

Figure S9B

TSD-HE for assessing histological characteristics in liver cancer

Table S1

Δ

Figure 4A-B

Figure 3H

Figure 4B

Figure 4G

P **Figure 4H**

Figure 4I

Figure 4C-D and S11

Figures 4B-C

Figure 4J

Figure 4B-C

Figure 4B
Figure 4C **Figure S11C, I**

Figure S12

Figure 4E and S13A

P
Figure 4F

P **Figure 4F** Δ **Figure S13B**

Figure S13C

TSD-HE for surgical specimen diagnosis of esophageal carcinoma, cholangiocarcinoma, and pancreatic cancer

Esophageal carcinoma.

Table S1

Figure S14A

Figure S14B-D

Cholangiocarcinoma and pancreatic cancer.

Table S1

Table S1

Figure 5

Figure

1A and S4C-D, G

Figure 5A-D

Figure 5B

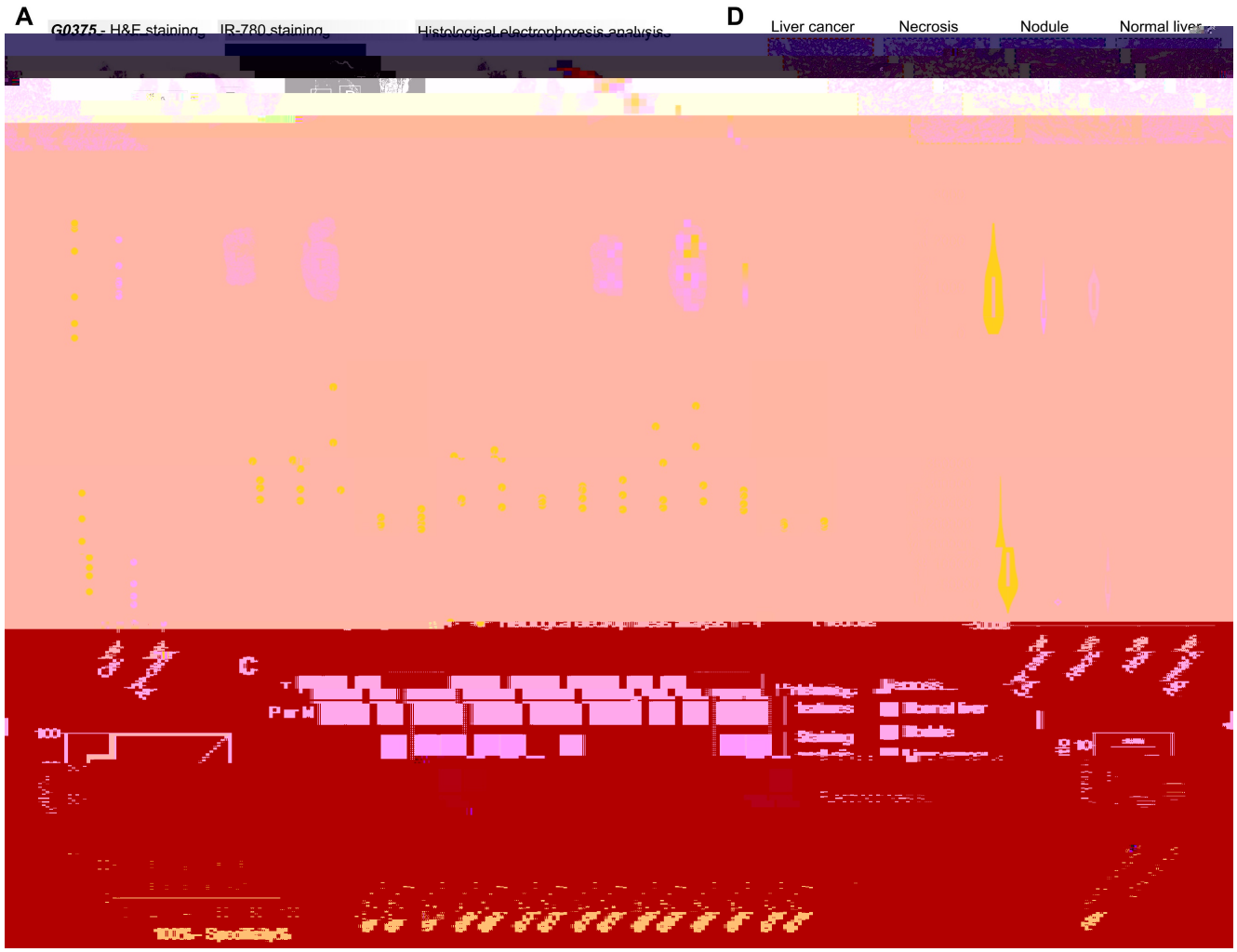

Figure 4. Signals of IR-780-labeled proteins reflect histological characteristics in liver cancer. (A) Compared to IR-780-based staining analysis, IR-780-based histological electrophoresis analysis faithfully represents the distribution of histological types in tissue sections. (B) Enhancement of tumor-to-paracancerous (or normal) tissue ratios in liver cancer via histological electrophoresis analysis. The specimens of liver cancer are obtained from nine patients (**Table S1**). (C) Association between tumor-to-paracancerous (or normal) tissue ratios and the histological types of tumor and paracancerous (or normal) tissue. (D) H&E staining results reflect four representative histological types (liver cancer, necrosis, liver nodule, and normal liver) in the surgically resected tissue of liver cancer. Scale bar: 500 μm. (E and F) Violin plots show the signal distribution after staining analysis (E) and histological electrophoresis analysis (F) in liver cancer and several normal tissue types across multiple patients (n = 9). Statistical significance is calculated using a *t*-test: **P* = 0.0290 and *****P* < 0.0001. (G and H) The patient-wise (n = 9) mean signal intensity of cancer (orange) and non-cancer tissue (purple), calculated as the mean of multiple ROIs (For staining analysis, the number of ROIs is five, and the size of ROIs is 1 mm × 1 mm, G; for histological electrophoresis, n > 10, H) of histologically identified cancer and non-cancer tissue. Statistical significance is calculated using a *t*-test: ***P* = 0.0068. (I) Comparison of the ratios calculated from the IR-780-staining strategy and IR-780-based electrophoresis separating strategy. Significant differences are observed between the covalent binding group and the non-specific adsorption group. (****P* = 0.0004). (J) ROC plot of sensitivity% versus 100%-specificity% for cancer versus non-cancer classification in data from specimens across the above patients. The AUC is 0.92 for histological electrophoresis analysis versus 0.55 for staining analysis.

Figure 5E-H

Figure 5E-H

Figure 5F Figure 5F

Figure 5. Distinguishing tumors from normal tissues in cholangiocarcinoma and pancreatic cancer surgical specimens using TSD-HE. (A) Cholangiocarcinoma at different primary locations and the corresponding clinical resection range (pancreaticoduodenectomy for G0235 and cholangiocarcinoma resection for G0329). (B) Comparison of IR-780-based staining analysis and IR-780-based histological analysis in the cholangiocarcinoma specimens from above patients. (C and D) Photographs and H&E staining results of flesh resected cholangiocarcinoma specimens obtained from G0235 (C) and G0329 (D). Scale bar: 500 μm. Dashed lines indicate the

clinically identified tissue boundary. (E) Pancreatic cancer at different primary locations and the corresponding clinical resection range (partial pancreatectomy for G1172 and pancreaticoduodenectomy for G0241). (F) Comparison of IR-780-based staining analysis and IR-780-based histological analysis in the pancreatic cancer specimens from above patients. (G and H) Photographs and H&E staining results of flesh resected pancreatic cancer specimens are obtained from G1172 (G) and G0241 (H). Scale bar: 500 μm. Dashed lines indicate the clinically identified tissue boundary.

Figure 5

P

Figure 6A and S15

Figure S16

(Δμ **Figure 6F**

Figure S15A, D

Comparison of TSD-HE diagnosis and clinical pathological diagnosis

Figure S15C-D

Figure 6G **Figure 6F**

Figure 6H

Figure 6I

Figure 6B

Figure 6C **Figure S17** **Figure S17**

Figure 6D-E

Δ

Figure 6D

Figure 6H and S18A-C
Figures 6I and S18D

(Δμ **Figure 6D**

Δ

Figure 6E

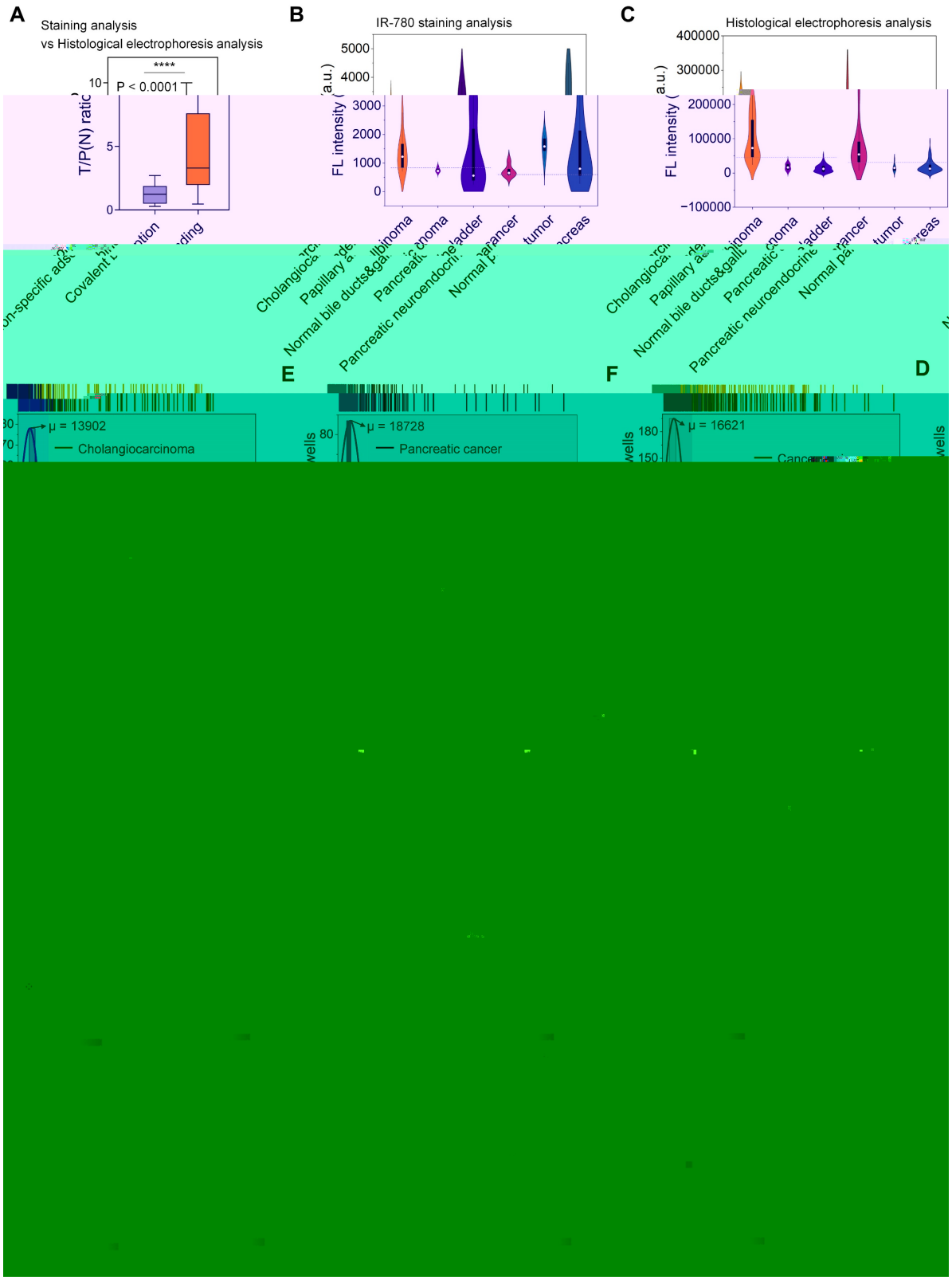

Figure 6. Signals of IR-780-labeled proteins reflect histological characteristics in cholangiocarcinoma and pancreatic cancer. (A) Comparison of the ratios calculated from IR-780-staining strategy and IR-780-based electrophoresis separating strategy. Significant differences are observed between the covalent binding group and the non-specific adsorption group. (****$P < 0.0001$). (B and C) Violin plots show the signal distribution after staining analysis (B) and histological electrophoresis analysis (C) in cholangiocarcinoma, pancreatic cancer, and several normal tissue types across multiple patients (n = 14). (D-F) Histograms of the covalent binding signals of different histological types within cholangiocarcinoma and pancreatic cancer tissue sections. (D) Histological types within the tissue sections from the above cholangiocarcinoma patients include: cholangiocarcinoma, normal bile duct and gallbladder, and papillary adenoma. (E) Histological types within the tissue sections from the above pancreatic cancer patients include: pancreatic cancer, pancreatic neuroendocrine tumor, and normal pancreas. (F) Signal histogram of cancer regions and non-cancer regions from the surgical specimens of cholangiocarcinoma and pancreatic cancer. (G) Schematic representation of the workflow of TSD-HE analysis for tissue sections of surgical specimens. (H) Automatically diagnosis of cancer region in the cholangiocarcinoma surgical specimens (from G0065 and G0193) via signal threshold. (I) Automatically diagnosis of cancer region in the pancreatic cancer surgical specimens (from G1631 and G0534) via signal threshold.

Conclusions

Figure 1A and S4

Materials and Methods

Collection of clinical specimens and information

J

ICG-/IR-780-/IR-780Ac-based staining analysis of tissue sections

Structural and purity characterization of dyes

ICG-/IR-780-/IR-780Ac-based histological electrophoresis analysis of tissue sections

μm)

Structural and purity characterization of ICG

d δ *J*
J *J*
J *J*
J *J* μM
J

Structural and purity characterization of IR-780

d δ *J*
J *J*
J *J*

J

Structural and purity characterization of IR-780Ac

δ *J*
J
J *J*
J

μm.

H&E staining analysis

Lysis of tissues

g

ICG, IR-780, and IR-780Ac labeling of protein standards

β

Fluorescent probe labeling of tissue lysate

Sodium dodecyl sulfate-polyacrylamide gel electrophoresis (SDS-PAGE) analysis and gel imaging

Statistical analyses

P

Abbreviations

β β

Supplementary Material

Acknowledgements

Author contributions

Competing Interests

References